



Mechanical properties and interface toughness of metal filled nanoporous anodic aluminum oxide coatings on aluminum

J. Zechner^{a,*}, G. Mohanty^a, C. Frantz^a, H. Cebeci^b, L. Philippe^a, J. Michler^a

^a EMPA, Swiss Federal Laboratories for Materials Science and Technology, Laboratory for Mechanics of Materials and Nanostructures, Feuerwerkerstrasse 39, 3602 Thun, Switzerland

^b Rero AG, Hauptstrasse 96, 4437 Waldenburg, Switzerland

ARTICLE INFO

Available online 21 September 2014

Keywords:

Anodic aluminum oxide
Interface toughness
Mechanical interlocking
Micro-cantilever
Nanoindentation

ABSTRACT

The mechanical properties and coating/substrate interface toughness of nanoporous anodic aluminum oxide thin films, both unfilled and metal-filled, are investigated in the current study. A two-step anodization process is used to grow the porous oxide, which is subsequently filled with Ni. The mechanical properties of the coating are probed using nanoindentation and the micro-cantilever deflection technique is used to study the interface toughness. The results are discussed and suggestions for improving the interface toughness are made.

© 2014 Elsevier B.V. All rights reserved.

1. Introduction

In the present study, the suitability of nanoporous anodic aluminum oxide (AAO) as the base layer for metallic coatings on aluminum is investigated. Due to its unique honeycomb like structure consisting of regular nanopores that can be filled with different metallic, ceramic or polymeric materials, AAO has been intensively investigated as an attractive material for various applications in optics, electronics and magnetism in recent years [1]. The nanoporous structure can also be used as an attractive base layer for coatings on aluminum and its alloys, especially in cases where the layer adhesion on the substrate is critical for a successful application. Thus, it could also be used as an alternative to the zincate-plating process [2], in which a zinc layer is produced by galvanic displacement of aluminum with zincate. This zinc layer prevents further oxidation of aluminum and serves as substrate for subsequent metallizations. Although it has been in use for many decades, obtaining well adhering coatings using the zincate process is still challenging and leads to high rejection rates in production. Therefore, there is a strong industrial demand for an alternative process with improved process control.

The basic idea of this work is to grow an anodic alumina layer with a regular nanoporous structure, which is afterwards filled with Ni. This should serve as an industrially relevant example for metallization on aluminum. The filled porous structure should then act as a mechanical anchor for the film on the substrate. This strategy is known to have an advantageous influence on coating adhesion [3]. Therefore, in the current study, an AAO layer is grown on a high purity aluminum substrate,

which is subsequently filled with Ni to form a nanocomposite thin film consisting of an alumina matrix filled with Ni nanowires. The mechanical properties of the coating are probed by nanoindentation and the toughness of the substrate/coating interface is quantitatively measured using the micro-cantilever deflection technique [4,5].

2. Experimental

2.1. Coating deposition

For film deposition, 0.5 mm thick Al disks (99.999%) are degreased in 1.25 N NaOH at 60 °C for 5 min, neutralized in 5.55 N HNO₃, and then electropolished in HClO₄:C₂H₅OH = 1:3 at 10 °C for 2 min at 20 V. Afterwards, a two-step anodization process is applied in order to obtain well organized nanopore arrays. The first anodization is achieved in 0.3 M H₂SO₄ at 3 °C for 8 h at 25 V. The obtained oxide layer is subsequently dissolved by immersion in 0.4 M H₃PO₄ + 0.2 M H₂CrO₄ at 60 °C for at least 1 h. The second anodization is carried out under the same conditions as the first one for 1800 s. Directly after that, the anodization potential is exponentially decreased down to 7.5 V through 60 steps of 20 s each, and finally maintained at 7.5 V for 600 s. This last step allows thinning and homogenizing the barrier oxide layer in order to facilitate subsequent electrodeposition.

Then, the porous anodic aluminum oxide is filled with Ni by potentiostatic reverse pulse deposition in 0.73 M H₃BO₃ containing 0.154 M Ni(NH₂SO₃)₂, 0.7 mM SDS and 10.9 mM saccharine at 45 °C. The potential waveform consists of a cathodic pulse of 8 ms at −11 V followed by a short anodic pulse of 2 ms at 7.5 V. This period is repeated 360,000 times. Al disks and chemicals are purchased from Goodfellow and Sigma-Aldrich respectively. A Julabo refrigerated/heating circulator

* Corresponding author.

E-mail address: johannes.zechner@empa.ch (J. Zechner).

F12-ED is used for accurate control of electrolyte temperature and all electrochemical experiments are conducted using a potentiostat/galvanostat Autolab PGSTAT302N equipped with a voltage multiplier.

2.2. Nanoindentation

Nanoindentation tests are performed on unfilled AAO and Ni-filled AAO using a Hysitron Ubi 1 system (Hysitron Inc., Minneapolis). A maximum load of 3 mN is applied to yield penetration depths of ~150 nm. The indentation depth is less than 10% of film thickness (of 2.6 µm) and well within the range to avoid substrate effect [6]. High sample roughness due to filling up and overflow of the AAO pores with Ni poses a challenge in terms of indenting flat surfaces and measuring the mechanical properties of the composite. Performing grid indents blindly would have resulted in undesirable artifacts in measurements due to the indenter tip landing on slant surfaces, indenting only Ni and large scatter in experimental data. This problem is tackled by performing surface topography scans using the indenter tip (SPM feature in this instrument) and placing the indents in relatively flat areas. This provides consistent results over a large region tested on the sample.

The recorded load–displacement data of all tests are evaluated using the Oliver–Pharr method [7]. The hardness and modulus values determined for AAO are for the overall porous structure. This is in contrast to the proposal by Ng et al. [8] to measure the true solid area of the residual indents, i.e. the gross indent area minus the area of the pores, in order to obtain the hardness of the solid AAO.

2.3. Fracture mechanics testing

For the cantilever fabrication, a Ni-filled AAO specimen is cut in half using a water cooled wire saw and low cutting speeds to minimize heating of the specimen. One of the halves is subsequently ground to achieve a flat cutting surface and afterwards mechanically polished using alumina suspension with a particle size of 0.25 µm. The surface layer, plastically deformed by polishing, is removed by focused ion beam (FIB) machining with a Tescan Lyra dual beam FIB/SEM workstation at 30 keV with 7 nA ion current. The free-standing microcantilevers are subsequently FIB milled with currents decreasing from 5 nA for coarse milling to 90 pA for fine polishing to reduce FIB damage. The nominal target size of the cantilevers is a length of $L = 3 \mu\text{m}$, a thickness of $B = 1 \mu\text{m}$ and a width of $W = 1 \mu\text{m}$, with the interface lying 0.4 µm from the cantilever base. The dimensions of each cantilever are measured after the last polishing step. Subsequently, a notch is introduced into the cantilevers directly at the interface using FIB machining at low ion current conditions (30 keV, 10 pA). Fig. 1 shows a sketch of the orientation of the cantilevers with respect to the coating structure.

The cantilevers are tested in-situ in a ZEISS DSM962 tungsten filament scanning electron microscope (SEM). An ALEMNIS microindenter with a 500 mN load cell and a spheroconical indenter (tip radius = 710 nm) are used for testing in displacement control with a

displacement rate of 3 nm/s. Cantilever bending inside the SEM allows easy positioning of the indenter on the cantilever, as well as the monitoring of deformation and the onset of crack growth on the specimen. The bending length l , i.e. the distance between the notch and the indenter contact point, is measured for each cantilever prior to testing. The load–displacement data are thermal-drift corrected by measuring the load change during a 300 s holding step applied both before and after testing. The load measured during the tests is offset by the loading rate determined in these holding steps. A total of 10 specimens are tested. Four samples show pronounced plastic deformation in the Al substrate at the cantilever base before crack growth initiation and are therefore not taken into account for the interface toughness measurement.

Post-mortem analysis of the fracture surfaces is conducted in a Hitachi S4800 high resolution SEM (HRSEM). The initial notch depth a of each cantilever is measured on the fracture surfaces and is $0.43 W < a < 0.55 W$.

The measured load F and notch length are used to calculate the fracture initiation toughness K_C according to [9]:

$$K_C = \frac{6Fl}{BW^2} \sqrt{\pi a} f\left(\frac{a}{W}\right), \quad (1)$$

with the dimensionless geometry factor

$$f\left(\frac{a}{W}\right) = \sqrt{\frac{2W}{\pi a} \tan \frac{\pi a}{2W} \frac{0.923 + 0.199(1 - \sin \frac{\pi a}{2W})^4}{\cos \frac{\pi a}{2W}}}. \quad (2)$$

The resulting K_C is converted into an energy release rate G_C using the relationship

$$G_C = \frac{K_C^2}{E^*}, \quad (3)$$

with [10]

$$\frac{1}{E^*} = \frac{1}{2} \left(\frac{1}{E_F} + \frac{1}{E_s} \right). \quad (4)$$

Here E_F is the film's Young's modulus determined using nanoindentation and $E_s = 70 \text{ GPa}$ is the Young's modulus of the Al substrate.

3. Results

A top-view HRSEM image of the unfilled AAO structure is given in Fig. 2a. The islands visible on the top of the AAO stem from coating the film with gold to prevent charging. A FIB-machined cross-section of the Ni-filled coating is shown in Fig. 2b, with a magnified view of the interface area shown in Fig. 2c. The thickness of the coating is 2.6 µm. The bright lines ranging from the substrate to the top of the coating (Fig. 2b, c) are the metallic Ni nanowires filling the porous AAO structure. The metallic nature of the nanowires is also confirmed by XRD measurements, from which an average grain size of 30 nm is calculated using the Scherrer equation (not reported in this manuscript). Using HRSEM, the pore diameter is determined to be around 28 nm and the interpore distance to be about 65 nm, which results in a porosity $V_p = 14.8\%$ and a pore density of $2.4 \times 10^{10} \text{ cm}^{-2}$ in the film plane. The cross-section reveals that not all pores are completely filled with Ni. Furthermore, a thin continuous alumina barrier layer is found at the interface between the aluminum substrate and the porous AAO.

The results of the nanoindentation measurements are given in Table 1. For the unfilled AAO, the indentation hardness H_{AAO} are $4.4 \pm 0.3 \text{ GPa}$ and $113.4 \pm 3.3 \text{ GPa}$, respectively. The hardness H_F and Young's modulus E_F of the film consisting of Ni-filled AAO are $4.4 \pm 0.7 \text{ GPa}$ and $101.4 \pm 8.9 \text{ GPa}$.

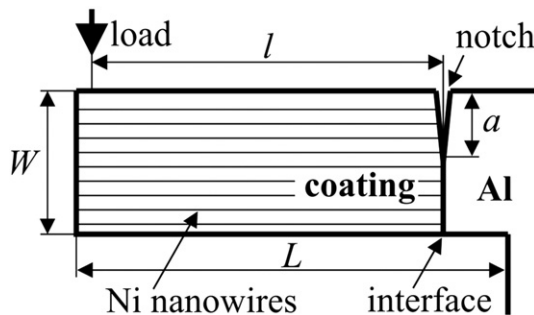


Fig. 1. Sketch of the cantilever orientation with respect to coating orientation and denominations.

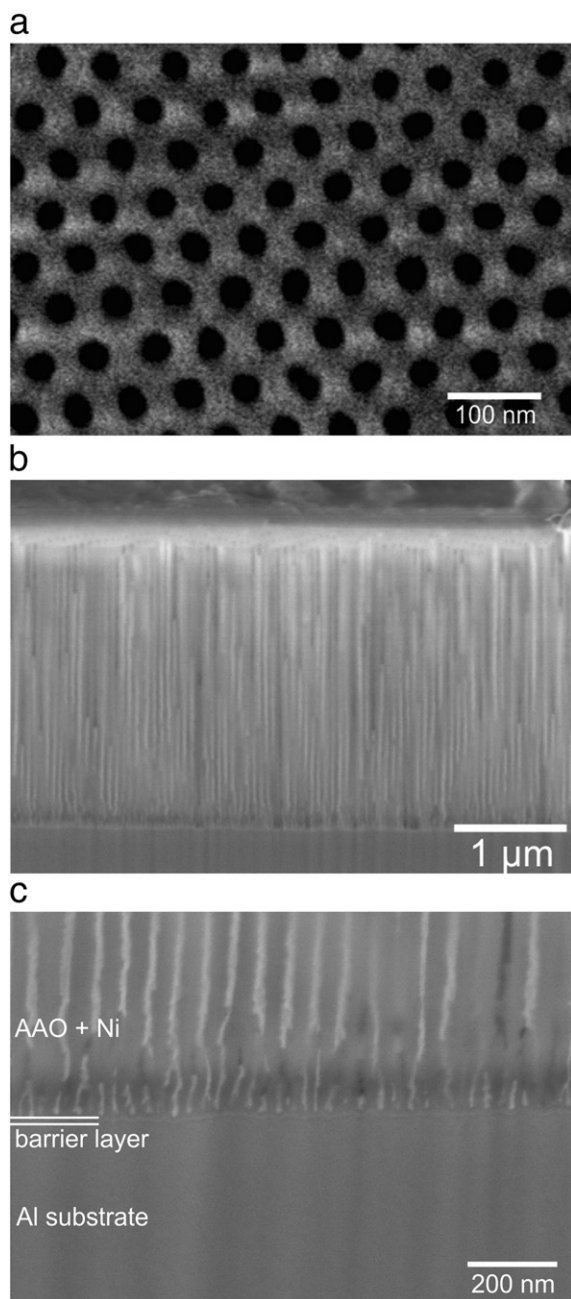


Fig. 2. Top-view of the unfilled nanoporous AAO (a). Cross-section of the Ni-filled AAO structure (b). Magnified view of the interface structure of the Ni-filled coating (c).

The drift-corrected load–displacement curves of several fracture mechanics tests are shown in Fig. 3a. The curves of all tests show an initial linear increase of load with displacement. Upon crack growth initiation, which is observable during in-situ testing, the load–displacement curves deviate from linear behavior and the slope decreases strongly. The load at the point of this deviation, indicated with arrows in Fig. 3a, is used for the calculation of K_{IC} together with the initial

Table 1
Young's moduli as well as hardness of the unfilled AAO and Ni-filled AAO film.

	Young's modulus [GPa]	Hardness [GPa]
Unfilled AAO	113.4 ± 3.3	4.4 ± 0.3
Ni-filled AAO	101.4 ± 8.9	4.4 ± 0.7

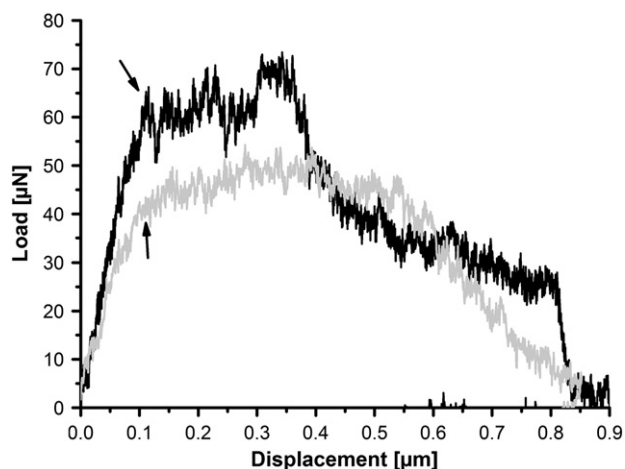


Fig. 3. Load–displacement-curves obtained from the microcantilever bending experiments. The arrows indicate the point of crack growth initiation.

crack length determined post-mortem according to Eq. (1). The cantilevers do not break off the base material but a short ligament remains intact after testing, see Fig. 4a. For the six successful tests, K_{IC} is determined to be $1.1 \pm 0.25 \text{ MPam}^{0.5}$. Inserting E_F and E_s into Eq. (4) and applying Eq. (3) gives an average energy release rate G_C of 14.9 J/m^2 .

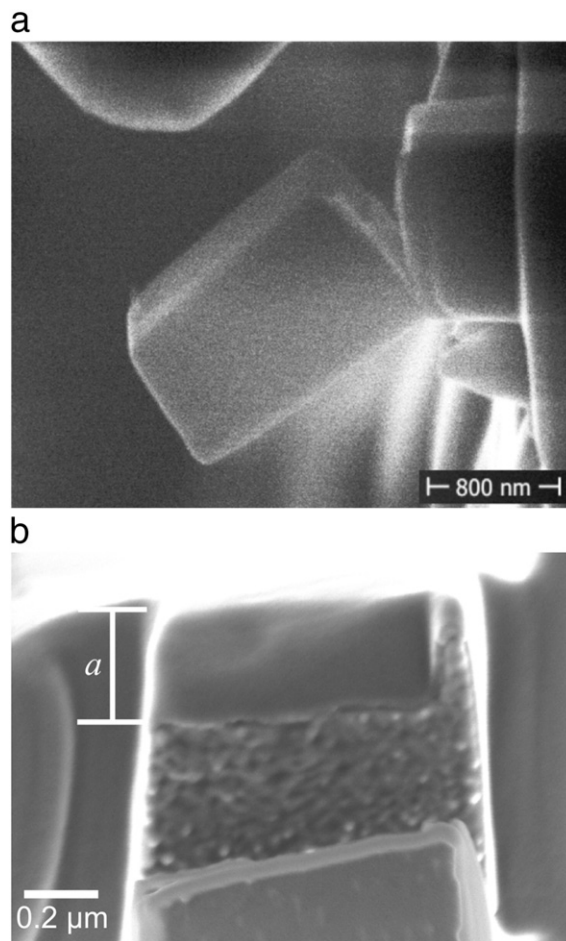


Fig. 4. SEM image of a microcantilever after testing (a) and fracture surface of the cantilever; the upper part shows the FIB-notch (length a) whereas the lower structure is caused by stable crack growth (b).

4. Discussion

The HRSEM image and FIB cross-sections through the Ni-filled AAO film (see Fig. 2a–c) show a very regular and fine porous AAO structure. The mechanical properties of the unfilled AAO lie well within the range of values reported in literature, which range from 122 GPa < E_{AAO} < 140 GPa and 7 GPa < H_{AAO} < 8.5 GPa for dense AAO thin films [11,12], to $E_{\text{AAO}} = 3$ GPa and $H_{\text{AAO}} = 0.3$ GPa for AAO with 60% porosity (200 nm pore diameter) [13]. According to Bert [14], the Young's modulus of dense material (E_{dense}) can be estimated from the Young's modulus measured on a sample containing cylindrical pores oriented parallel to the loading axis (E_{porous}) using

$$E_{\text{dense}} = \frac{E_{\text{porous}}}{1 - V_p} \quad (5)$$

Inserting $E_{\text{AAO}} = 113.4$ GPa for E_{porous} and porosity $V_p = 14.8\%$ into Eq. (5) gives the estimation of the Young's modulus for dense AAO $E_{\text{AAO,dense}} = 133$ GPa, which agrees well with the values measured for dense AAO given above. It is interesting to notice that due to the amorphous structure of the dense AAO, the Young's modulus is only about one third of that of polycrystalline alumina (416 GPa [15]).

The mechanical properties of Ni filled AAO have not been reported in literature yet, which prevents a direct comparison of the measured values with similar coating structures. Xia et al. [16] conducted nanoindentation experiments on AAO filled with carbon nanotubes (CNT) and measured Young's moduli ranging from 134 GPa for a 20 μm thick coating with a pore diameter of 53 nm to 87 GPa for a 90 μm thick film with a pore diameter of 70 nm. The hardness of the CNT-filled AAO was determined to be 6.9 GPa for the thin coating and 4 GPa for the thicker coating. Taking into account the different mechanical properties of the filler materials, the different pore diameter and possible differences in the AAO properties caused by electrodeposition, it can be concluded that the E_F values measured in this study lie in a comparable range and seem reasonable. An estimation of the composite properties from the properties of the constituent materials using a rule of mixtures is not practical due to the strong anisotropy of the constituents and the unknown mechanical properties of the Ni nanowires, which can strongly differ from those of bulk electrodeposited Ni.

An interesting point here is that the hardness of the AAO is unaffected by the filling with Ni and that the Young's modulus even slightly decreases upon Ni-filling (see Table 1). This behavior is contradictory to what would be expected from the classical rule of mixture estimations for fiber reinforced composites. An identical behavior is also reported in [16] for the CNT filled AAO, where the hardness does not change and the Young's modulus decreases by 20% upon CNT-filling. A possible explanation for this material behavior could lie in the Young's modulus measurement methodology using nanoindentation. As usual, the Young's moduli of the unfilled and Ni-filled AAO are determined from the compliance of the unloading part of the load–displacement curve. HRSEM images have been made of the nanoindentations in unfilled AAO, which show that the open pore structure collapses in the vicinity of the indenter, an effect which has also been described in [17]. Thus, a densification of the material, i.e. a decrease in porosity V_p , occurs during the loading phase of the indentation measurement. Therefore, the compliance of the unloading curve corresponds to that of a material with less porosity, which has a higher Young's modulus, compare Eq. (5). If the filling of the pores prevents this densification and does not increase the Young's modulus itself, the porous structure might have a higher apparent Young's modulus than the filled one. Another explanation could be that the AAO structure is altered by electrochemical processes during the electrodeposition of Ni. Investigating this effect would be an interesting point for future work on the deformation behavior of filled nanoporous alumina.

Similar to mechanical properties, no data for the interface toughness of metal-filled AAO on aluminum is available to allow a comparison with $K_C = 1.1$ MPa $\text{m}^{0.5}$ and $G_C = 14.9$ J/m 2 measured in this study. Therefore, the data is compared to interface toughness measurements conducted on Al coatings on alumina substrates, an intensively studied thin film system. Schneider et al. [18] measured the interface toughness of a 500 nm sputtered Al layer on alumina using the superlayer indentation technique [19,20] and determined $G_C = 5.6$ J/m 2 , which is significantly lower than the values determined in this study. In the overview article by Volinsky et al. [21], the results of the interface toughness measurements of various authors for Al thin films on Al_2O_3 substrates are summarized. G_C values ranging from 4 J/m 2 to 12 J/m 2 are found for Al layer thicknesses ranging from 200 nm to 2 μm , with a clear trend for increasing toughness with increasing layer thickness. This increase originates in the increase in the plastically deforming volume in front of the crack tip, which dissipates energy and thus leads to an effective increase in fracture resistance of brittle/ductile coating systems [22]. In the present Al/AAO + Ni coating system, the microcrystalline Al substrate is softer than the nanocrystalline coatings described above, which allows for more pronounced plastic deformation in front of the crack tip and can therefore explain the higher G_C values determined here. Also the difference in coating growth technique, anodization in this study and sputtering in [21], influences the interface toughness. Therefore, it can be concluded that $G_C = 14.9$ J/m 2 is a reasonable value for the interface toughness of the tested system. Additional interface toughness measurements on industrially applied metallizations on Al using the zincate process would help to get an idea if the presented technique is suitable as a replacement for such techniques.

In Fig. 4a one of the microcantilevers is shown after testing. Fig. 4b shows a HRSEM image of the fracture surface of the base of the cantilever and the tilted cantilever can be seen in the front. The upper part of the fracture surface shows the notch introduced by FIB milling. A rough, dimple like structure is visible on the fracture surface created by a stable crack growth. For the crack growth in the vicinity of Al/alumina interfaces, different crack paths have been reported in literature. In [23,24] it was found that cracks in this material combination generally grow parallel to the interface, either in the Al or Al_2O_3 , but not directly at the interface. Some brighter spots inside the dimple structure in Fig. 4b, caused by the material contrast of the secondary electrons, suggest the presence of a second phase on the fracture surface. This leads to the assumption that the crack grows along the base of the nanopores, just above the continuous alumina barrier layer which covers the surface. Fig. 2c shows a high magnification image of the interface area and a side-view of the dimple-like structure present at the bottom of the pores. In the present case, this crack path could be favorable as not all of the pores are filled with Ni and the present voids could act as flaws from which the crack can easily propagate. Thus, an improved filling of the pores should lead to an improvement of the interface toughness. Furthermore, a complete removal of the barrier layer during anodization could lead to metal–metal contact at the interface, which could also contribute to a better interface toughness and should be studied in the future.

5. Conclusion

The mechanical properties and interface toughness of unfilled and Ni-filled nanoporous anodic alumina are measured in the present work. For the unfilled porous anodic alumina, the Young's modulus and hardness are determined as 113.4 GPa and 4.4 GPa respectively. The Young's modulus of the composite coating is 101.4 GPa and the hardness is 4.4 GPa, both determined by nanoindentation. The interface toughness is measured using the microcantilever bending technique which results in a fracture toughness of 1.1 MPa $\text{m}^{0.5}$ and corresponds to a critical energy release rate of 14.9 J/m 2 . The values measured in

this work are consistent with the properties of comparable coatings found in the literature.

Acknowledgments

Financial support by the Swiss Commission for Technology and Innovation under project number 14697.1 PFIW-IW is gratefully acknowledged.

References

- [1] G. Kartopu, O. Yalcin, in: N. Lupu (Ed.), *Electrodeposited Nanowires Their Applications*, InTech, 2010.
- [2] K. Murakami, M. Hino, M. Hiramatsu, K. Osamura, T. Kanadani, *Mater. Trans.* 47 (2006) 2518–2523.
- [3] K.W. Allen, *Int. J. Adhes. Adhes.* 13 (1993) 67–72.
- [4] D. Di Maio, S.G. Roberts, *J. Mater. Res.* 20 (2005) 299–302.
- [5] K. Matoy, T. Detzel, M. Müller, C. Motz, G. Dehm, *Surf. Coat. Technol.* 204 (2009) 878–881.
- [6] R. Saha, W.D. Nix, *Acta Mater.* 50 (2002) 23–38.
- [7] W.C. Oliver, G.M. Pharr, *J. Mater. Res.* 7 (1992) 1564–1583.
- [8] K.Y. Ng, Y. Lin, A.H.W. Ngan, *Acta Mater.* 57 (2009) 2710–2720.
- [9] H. Tada, P.C. Paris, G.R. Irwin, *Stress Analysis of Cracks Handbook*, ASME Press, 2000.
- [10] J.W. Hutchinson, Z. Suo, *Adv. Appl. Mech.* 29 (1992) 63–191.
- [11] G. Alcalá, P. Skeldon, G.E. Thompson, A.B. Mann, H. Habazaki, K. Shimizu, *Nanotechnology* 13 (2002) 451–455.
- [12] G. Alcalá, S. Mato, P. Skeldon, G.E. Thompson, A.B. Mann, H. Habazaki, et al., *Surf. Coat. Technol.* 173 (2003) 293–298.
- [13] T.-H. Fang, T.H. Wang, C.-H. Liu, L.-W. Ji, S.-H. Kang, *Nanoscale Res. Lett.* 2 (2007) 410–415.
- [14] C.W. Bert, *J. Mater. Sci.* 20 (1985) 2220–2224.
- [15] R.G. Munro, *J. Am. Ceram. Soc.* 80 (1997) 1919–1928.
- [16] Z. Xia, L. Riestler, W. Curtin, H. Li, B. Sheldon, J. Liang, et al., *Acta Mater.* 52 (2004) 931–944.
- [17] Z. Xia, L. Riestler, B. Sheldon, W. Curtin, *Rev. Adv. Mater.* 6 (2004) 131–139.
- [18] J.A. Schneider, S.E. Guthrie, M.D. Kriese, W.M. Clift, N.R. Moody, *Mater. Sci. Eng. A* 259 (1999) 253–260.
- [19] M.D. Kriese, W.W. Gerberich, N.R. Moody, *J. Mater. Res.* 14 (1999) 3007–3018.
- [20] M.D. Kriese, W.W. Gerberich, N.R. Moody, *J. Mater. Res.* 14 (2011) 3019–3026.
- [21] A.A. Volinsky, N. Moody, W. Gerberich, *Acta Mater.* 50 (2002) 441–466.
- [22] V. Tvergaard, J.W. Hutchinson, *J. Mech. Phys. Solids* 41 (1993) 1119–1135.
- [23] J.M. McNaney, R.M. Cannon, R.O. Ritchie, *Acta Mater.* 44 (1996) 4713–4728.
- [24] B.J. Dalgleish, K.P. Trumble, A.G. Evans, *Acta Metall.* 37 (1989) 1923–1931.